Journal of Alloys and Compounds 509 (2011) L26–L29

Contents lists available at ScienceDirect

Journal of Alloys and Compounds

journal homepage: www.elsevier.com/locate/jallcom

Letter

TiO_2–g-C_3N_4 composite materials for photocatalytic H_2 evolution under visible light irradiation

Hongjian Yan*, Haoxin Yang

College of Chemistry, Sichuan University, Chengdu 610064 PR China

ARTICLE INFO

Article history:
Received 22 July 2010
Received in revised form
25 September 2010
Accepted 28 September 2010
Available online 8 October 2010

Keywords:
Semiconductors
Photocatalysis
Titanium dioxide
g-C_3N_4

ABSTRACT

In this investigation, we report the preparation of TiO_2–g-C_3N_4 composite materials with varying the wt.% of g-C_3N_4, the characterization of these materials by various techniques and photocatalytic hydrogen production under visible light irradiation in the presence of methanol. The X-ray powder diffraction (XRD) shows that the composite materials are consist of anatase TiO_2 and g-C_3N_4. Fourier transform infrared (FT-IR) spectra show that the absorbance band intensity of composite materials was stronger than that of C_3N_4. The UV–vis absorption spectra show that the absorption edge of the composite materials shifts to the lower energy region comparing to pure anatase and to longer wavelengths with increasing the amount of C_3N_4. The significant photoluminescence quenching was observed in TiO_2–C_3N_4 composite materials, indicating the charge transfer from C_3N_4 to TiO_2. The visible light induced H_2 evolution rate was remarkably enhanced by coupling TiO_2 with C_3N_4.

1. Introduction

Photocatalytic water splitting to produce hydrogen has become an area of great research interest because of the global energy crisis and environmental pollution since Fujishima and Honda first reported the decomposition of water on illuminated TiO_2 electrodes in 1972 [1]. To date, a variety of photocatalysts constructed from transition-metal ions with d_0 electronic configuration or post-transition-metal ions of d_{10} configuration, along with group VA or VIA ions as counter-anion components [2–6] have been developed. Among various kinds of photocatalysts, TiO_2 is widely used due to its optical and electronic properties, long-term stability, low cost, and nontoxicity. However, TiO_2 could only respond to UV irradiation that takes up ~4% of solar energy, which limits the application to a great extent. In the past decades, numerous methods have been developed to increase the photocatalytic efficiency of TiO_2, such as doping of TiO_2 with metallic (Cr, Fe, V) [7,8], and nonmetallic elements (N, C, B) [9,10] to increase the visible light absorbance, and coupling with other semiconductors [11–13] to increase the separation efficiency of photogenerated electron - hole pairs during photocatalysis.

Recently, Wang et al. [14] reported that a polymer semiconductor on the basis of a defecteous graphitic carbon nitride (g-C_3N_4) possesses the performance of hydrogen or oxygen production from water splitting under visible light irradiation in the presence of sacrificial donor or acceptor. The optical band gap of this polymer semiconductor was determined to be 2.7 eV. The g-C_3N_4 photocatalyst is considered to be stable under light irradiation in water solution as well as in acid (HCl, pH 0) or base (NaOH, pH 14) solutions due to the strong covalent bonds between carbon and nitride atoms. Very recently, a composite photocatalyst of g-C_3N_4 and TaON with visible light response was prepared by a milling-heat treatment method and was used for photodegradation of rhodamine B [15]. However, the photocatalytic activity is still low. Therefore it is expected to further improve the photocatalytic performance of g-C_3N_4 for obtaining more effective catalyst.

In this study, the preparation of TiO_2–g-C_3N_4 composite materials with varying the wt.% of g-C_3N_4, characterization of these materials by various techniques and photocatalytic hydrogen production under visible light irradiation in the presence of methanol are reported.

2. Experimental

All starting materials were purchased from commercial sources and were used without further purification.

The TiO_2 powders were prepared as follows: an aqueous solution of $TiCl_4$ (200 mL, 0.5 mol dm^{-3}) was added slowly to ammonia solution (200 mL, 2 mol dm^{-3}) under vigorous stirring. After stirred for 30 min the resulting slurry was filtered, washed with water and ethanol subsequently, filtered again, and kept under vacuum at 400 K for 12 h. Then the powders were calcined at 650 °C in air for 2 h.

The g-C_3N_4 was prepared by directly heating melamine under a flow of Ar gas. A quartz tube, 30 mm in inner diameter and 1000 mm in length, was used as a reaction chamber. In the synthesis, analytical grade melamine powder (10 g) was pressed into a semiclosed cylindrical quartz tube and then placed in the middle region of the reaction chamber. The quartz tube was heated to 380 °C in 5 min and then heated to 600 °C in a muffle furnace for 4 h at a heating rate of 1 °C min^{-1} in the flow of Ar

* Corresponding author. Tel.: +86 28 85221339; fax: +86 28 85221339.
E-mail address: hjyan@scu.edu.cn (H. Yan).

0925-8388/$ – see front matter © 2010 Elsevier B.V. All rights reserved.
doi:10.1016/j.jallcom.2010.09.201

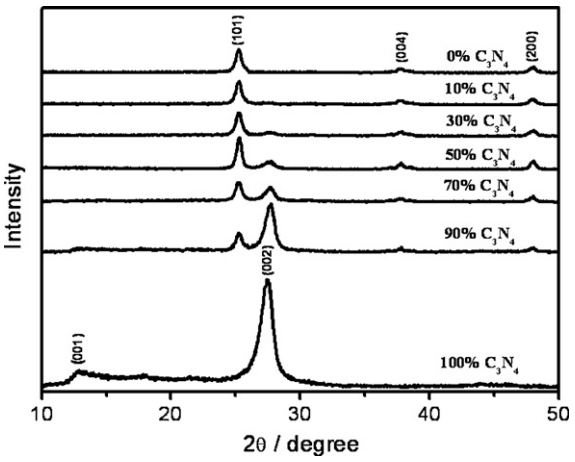

Fig. 1. The powder XRD patterns of C_3N_4, TiO_2 and TiO_2–C_3N_4 composite.

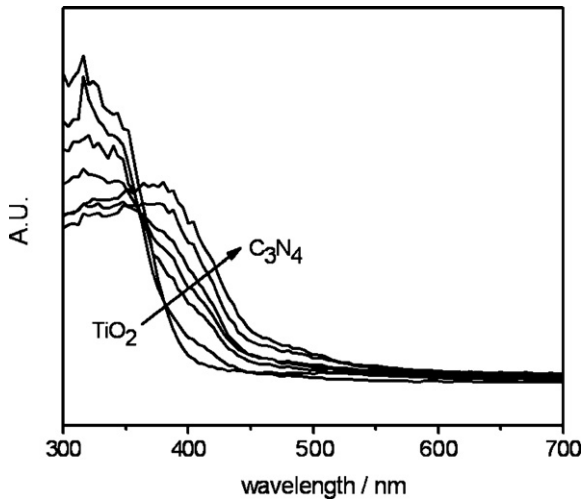

Fig. 3. The UV–vis absorption spectra of C_3N_4, TiO_2 and TiO_2–C_3N_4 composite materials.

gas. After the reaction, the quartz tube was cooled down to room temperature in the flow of Ar gas.

The TiO_2 and C_3N_4 powder were mixed by ball-milling and then calcined at 400 °C for 1 h in a muffle furnace.

The structural properties of the materials were analyzed by X-ray powder diffraction (XRD) on a X-Pert Pro diffractionmeter with CuKα radiation (λ = 1.5406 Å) at a scanning speed of 4° min^{-1}. FT-IR measurements were performed using a Fourier transform infrared (FT-IR) spectrometer (Nicolet 670) only in the mid infrared range of the instrument (400–4000 cm^{-1}) for samples dispersed in KBr pellets in 1:99 ratio. UV–vis diffuse reflection spectra were measured using a UV–vis spectrophotometer (UV2100, Shimadzu) and converted from reflection to absorbance by the Kubelka–Munk method. The photoluminescence measurements were performed in a luminescence spectrophotometer (Hitachi F-7000) operated at room temperature. The morphology of the composite materials was characterized using JEM-100CX Transmission Electron Microscopy (TEM, JEOL, Japan).

The photocatalytic reaction under visible light irradiation was carried out in an inner irradiation quartz cell (500 mL). The reaction cell was connected to a closed gas circulation system and the gases evolved were analyzed with an on-line TCD gas chromatograph (SPSIC, GC-102AT, argon carrier). In a typically photocatalytic reaction, 0.3 g of C_3N_4–TiO_2 powder was suspended in 400 mL of aqueous methanol solution (H_2O: CH_3OH = 7:1, in volume). 0.5 wt.% Pt cocatalyst was loaded on the photocatalyst powder by an in situ photodeposition method to promote H_2 production: under light irradiation, an equivalent molar amount of H_2PtCl_6 in solution was reduced to the metallic state and deposited onto the surface of the catalyst, forming the Pt-loaded catalyst. A 450 W high-pressure mercury lamp was blocked by a $NaNO_2$ aqueous solution (2 M) filled in quartz tube. In this case, it is considered that an emission of a high-pressure mercury lamp at 436 nm mainly contributes for the reaction.

3. Results and discussion

Fig. 1 shows the powder XRD patterns of C_3N_4, TiO_2 and TiO_2–C_3N_4 composite. Two pronounced peaks were found in g-C_3N_4 at 27.4° and 13.1°, which can be indexed to (0 0 2) and (0 0 1) diffraction planes of the graphite-like carbon nitride [16] and correspond to the characteristic interplanar staking peak of aromatic systems and the inter-layer structural packing, respectively. No impurity phase was observed in the TiO_2 sample, which is consistent with the XRD pattern of anatase. The TiO_2–C_3N_4 sample presents a two-phase composition: C_3N_4 and TiO_2.

Fig. 2a and b shows the Fourier transform infrared (FT-IR) spectra of C_3N_4 and TiO_2–50 wt.% C_3N_4 respectively. The FT-IR spectra of the synthesized C_3N_4 show the features very similar to those of published results [17]. The absorption band near 1640 cm^{-1} is attributed to C–N stretching, while the three at 1240, 1320 and 1403 cm^{-1} to aromatic C–N stretching. The band near 808 cm^{-1} is attributed to out-of plane bending modes of C–N heterocycles. A broad band near 3140 cm^{-1} corresponds to the stretching modes of terminal NH_2 or NH groups at the defect sites of the aromatic ring [18]. The FT-IR spectra of TiO_2–50 wt.% C_3N_4 is similar to those of C_3N_4. However, the absorbance band intensity of TiO_2–50 wt.% C_3N_4 is stronger than that of C_3N_4, which indicts the formation of a composite between TiO_2 and C_3N_4.

The optical properties of the samples were investigated by UV–vis diffuse reflectance spectroscopy. Fig. 3 shows the UV–vis absorption spectra of C_3N_4, TiO_2 and TiO_2–C_3N_4 composite materials. The absorption edge of the TiO_2 sample occurs at ca. 390 nm, and the band gap energy is estimated to be about 3.18 eV. After coupled with C_3N_4, the absorption edge shifts to the lower energy region. We can also see that the absorption edges of the composite samples shift remarkably to longer wavelengths with increasing the amount of C_3N_4. The decrease in band gaps of the samples is

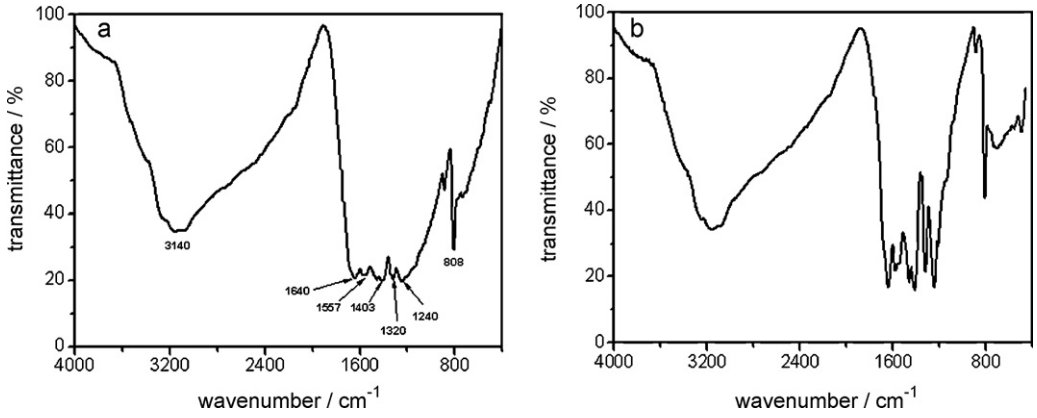

Fig. 2. The Fourier transform infrared (FT-IR) spectra of C_3N_4 (a) and TiO_2–50 wt.% C_3N_4 (b).

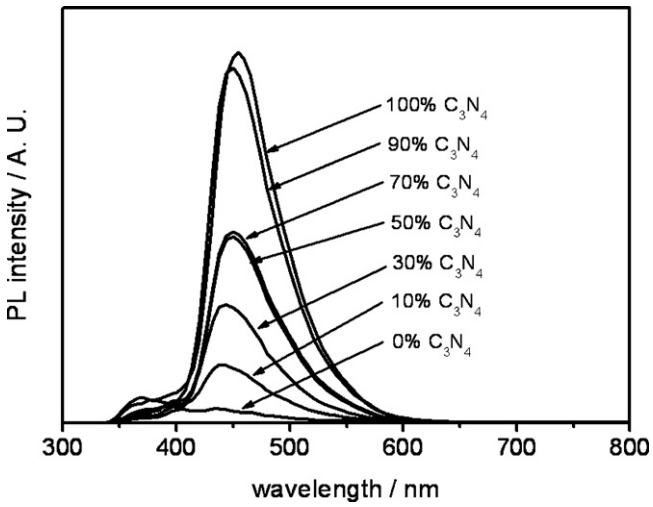

Fig. 4. The photoluminescence spectra of C_3N_4, TiO_2 and TiO_2–C_3N_4 composite materials.

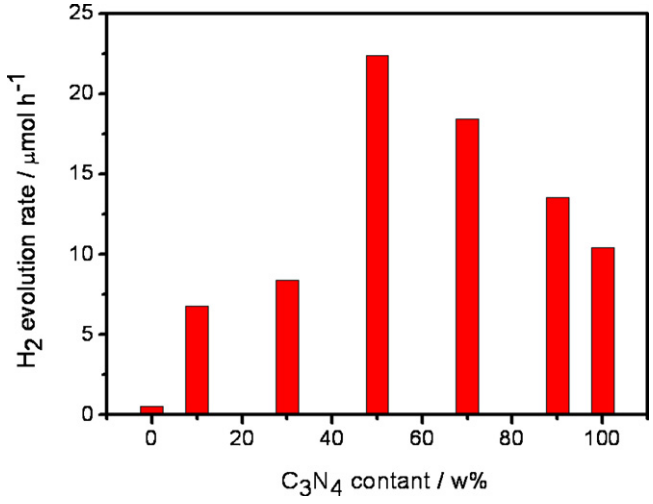

Fig. 5. The average hydrogen production rates as a function of wt.% C_3N_4 from the first 3 h of the reaction duration.

from 3.18 of TiO_2 to 2.68 eV of C_3N_4 when the content of C_3N_4 is increased from 0% to 100%.

Fig. 4 shows the photoluminescence (PL) spectra of the TiO_2–C_3N_4 composite materials. The peak at 453 and 369 nm could be related to electron-hole recombination of C_3N_4 and TiO_2, respectively. The significant PL quenching was observed in TiO_2–C_3N_4 composite materials as the content of TiO_2 increases. The quenching is due to the charge transfer occurs from C_3N_4 to TiO_2.

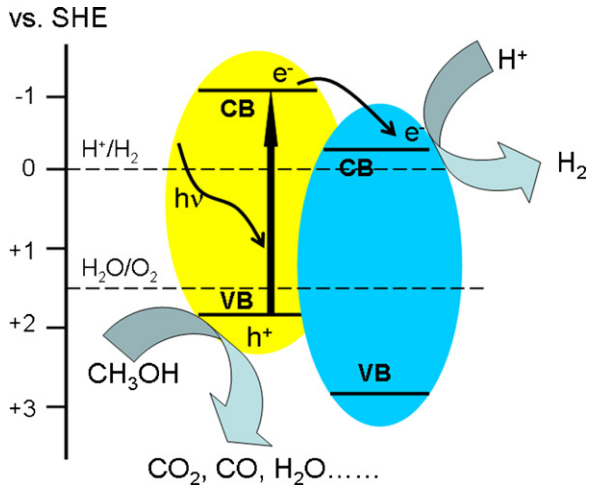

Fig. 7. The scheme for visible light-driven electron-hole separation of the TiO_2–C_3N_4 composite materials.

Photocatalytic hydrogen evolution from aqueous solutions containing CH_3OH (H_2O:CH_3OH = 7:1, in volume) was conducted under visible light using a 450 W high-pressure mercury lamp blocked by a $NaNO_2$ aqueous solution (2 M). Fig. 5 shows the average hydrogen production rates as a function of wt.% C_3N_4 from the first 3 h of the reaction duration. No hydrogen produced under the dark condition and without catalyst in presence of light. The evolution of hydrogen commenced after switching the lamp on in presence of catalyst only. However, the visible light induced H_2 evolution over TiO_2 is negligible. As shown in Fig. 5, the visible light induced H_2 evolution rate was remarkably enhanced by coupling TiO_2 with C_3N_4. Sample of TiO_2–50 wt.% C_3N_4 exhibits the highest activity with a hydrogen production rate of 22.4 μmol h^{-1}. The visible light induced H_2 evolution rate of TiO_2–50 wt.% C_3N_4 was 2 times of those of pure C_3N_4.

The morphology of TiO_2–50 wt.% C_3N_4 composite materials before and after photocatalytic reaction was investigated using TEM, as shown in Fig. 6(A) and (B) respectively. The particle size of the composite materials was estimated to be in the range of approximately 30–40 nm. After photocatalytic reaction, Pt nanoparticles with an average diameter of approximately 3–5 nm were deposited on the surface of the composite, which act as H_2 evolution site during photocatalytic reaction.

The enhancement of photocatalytic performance of the composite materials is attributed mainly to the effectively separation of photogenerated electron–hole pairs. Fig. 7 shows the scheme for visible light-driven electron-hole separation of the TiO_2–C_3N_4

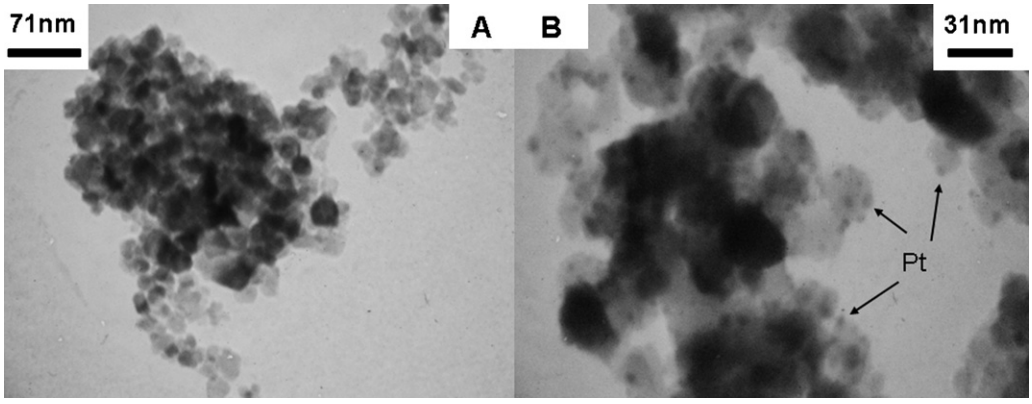

Fig. 6. The TEM images of TiO_2–50 wt.% C_3N_4 composite materials before (A) and after (B) photoreaction.

composite materials. The conduction band (CB) and valence band (VB) potentials of the TiO_2 and g-C_3N_4 are also shown in Fig. 7. The CB and VB edge potentials of g-C_3N_4 are at −1.12 and 1.57 eV, respectively [14]. The CB and VB edge potentials of TiO_2 are at −0.29 and 2.91 eV, respectively [19]. Since the CB edge potential of g-C_3N_4 (−1.12 eV) is more negative than that of TiO_2 (−0.29 eV) the photoinduced electrons on g-C_3N_4 particle surfaces transfer easily to TiO_2 via the well developed interface and reduce H^+ to H_2. However, the photoinduced holes were suspended in g-C_3N_4 due to the large difference in VB edge potentials and oxidize the sacrificial agent (CH_3OH) to products, such as CO_2, CO.

4. Conclusions

In summary, the TiO_2–g-C_3N_4 composite materials with varying the wt.% of g-C_3N_4 were prepared in this investigation. The composite materials present a two-phase composition: anatase TiO_2 and g-C_3N_4. The absorbance band intensity of composite materials is stronger than that of C_3N_4. The absorption edge of the coupling materials shifts to the lower energy region comparing to pure anatase and to longer wavelengths with increasing the amount of C_3N_4. The photocatalytic result show that the visible light induced H_2 evolution rate was remarkably enhanced by coupling TiO_2 with C_3N_4 due to the effectively separation of photogenerated electron-hole pairs.

Acknowledgments

We thank the Fundamental Research Funds for the Central Universities (Project No. 2009SCU11105) and Prof. Can Li for the financial support.

References

[1] A. Fujishima, K. Honda, Nature 238 (1972) 37–38.
[2] G. Hitoki, T. Takata, J.N. Kondo, M. Hara, H. Kobayashi, K. Domen, Chem. Commun. 16 (2002) 1698–1699.
[3] A. Ishikawa, T. Takata, J.N. Kondo, M. Hara, H. Kobayashi, K. Domen, J. Am. Chem. Soc. 124 (2002) 13547–13553.
[4] K. Maeda, T. Takata, M. Hara, N. Saito, Y. Inoue, H. Kobayashi, K. Domen, J. Am. Chem. Soc. 127 (2005) 8286–8287.
[5] K. Maeda, K. Teramura, D. Lu, T. Takata, N. Saito, Y. Inoue, K. Domen, Nature 440 (2006) 295.
[6] Y. Lee, H. Terashima, Y. Shimodaira, K. Teramura, M. Hara, H. Kobayashi, K. Domen, M. Yashima, J. Phys. Chem. C 111 (2007) 1042–1048.
[7] F. Lin, D.M. Jiang, X.M. Ma, J. Alloys Compd. 470 (2009) 375–378.
[8] J.J. Xu, Y.H. Ao, D.G. Fu, C.W. Yuan, Colloid Surf. A 334 (2009) 107–111.
[9] S.Z. Chen, P.Y. Zhang, D.M. Zhuang, W.P. Zhu, Catal. Commun. 5 (2004) 677–680.
[10] F. Dong, W.R. Zhao, Z.B. Wu, Nanotechnology 19 (2008) 365607.
[11] S.K. Poznyak, D. Talapin, A. Kulak, J. Phys. Chem. B 105 (2001) 4816–4823.
[12] Y. Liu, F. Xin, F. Wang, S. Luo, X. Yin, J. Alloys Compd. 498 (2010) 179–184.
[13] A. Dodd, A. McKinley, T. Tsuzukic, M. Saunders, J. Alloys Compd. 489 (2010) L17–L21.
[14] X. Wang, K. Maeda, A. Thomas, K. Takanabe, G. Xin, J.M. Carlsson, K. Domen, M. Antonietti, Nat. Mater. 8 (2009) 76–80.
[15] S.C. Yan, S.B. Lv, Z.S. Li, Z.G. Zou, Dalton Trans. 39 (2010) 1488–1491.
[16] S. Matsumoto, E.-Q. Xie, F. Izumi, Diamond Relat. Mater. 8 (1999) 1175–1182.
[17] K. Gibson, J. Glaser, E. Milke, M. Marzini, S. Tragl, M. Binnewies, H.A. Mayer, H.J. Meyer, Mater. Chem. Phys. 112 (2008) 52–56.
[18] L. Liu, D. Ma, H. Zheng, X.J. Li, M.J. Cheng, X.H. Bao, Microporous Mesoporous Mater. 110 (2008) 216–222.
[19] Y. Xu, M.A.A. Schoonen, Am. Mineral. 85 (2000) 543–556.